Fibrous meat analogues containing oat fiber concentrate and pea protein isolate: Mechanical and physicochemical characterization

Ramos-Diaz, Jose Martin

2022-05-22

Ramos-Diaz , J M , Kantanen , K A , Edelmann , M , Suhonen , H , Sontag-Strohm , T , Jouppila , K & Piironen , V 2022 , ' Fibrous meat analogues containing oat fiber concentrate and pea protein isolate: Mechanical and physicochemical characterization ' , Innovative Food Science and Emerging Technologies , vol. 77 , 102954 . https://doi.org/10.1016/j.ifset.2022.102954

http://hdl.handle.net/10138/341600
https://doi.org/10.1016/j.ifset.2022.102954

Innovative Food Science and Emerging Technologies 77 (2022) 102954

Contents lists available at ScienceDirect

Innovative Food Science and Emerging Technologies

journal homepage: www.elsevier.com/locate/ifset

Fibrous meat analogues containing oat fiber concentrate and pea protein isolate: Mechanical and physicochemical characterization

J.M. Ramos Diaz [a,*], K. Kantanen [a], J.M. Edelmann [a], H. Suhonen [b], T. Sontag-Strohm [a], K. Jouppila [a], V. Piironen [a]

[a] Department of Food and Nutrition, University of Helsinki, Agnes Sjöbergin katu 2, FI-00014 Helsinki, Finland
[b] Department of Physics, University of Helsinki, Gustaf Hällströmin katu 2, FI-00014 Helsinki, Finland

ARTICLE INFO

Keywords:
Oat
Pea
β-Glucan
Protein isolate
Meat analogues
High-moisture extrusion

ABSTRACT

A new generation of plant-based texturized meat analogues attempts to boost the consumption of dietary fiber. In the present study, oat fiber concentrate (OFC) and pea protein isolate (PPI) were combined (30:70; 50:50; 70:30) and processed with high-moisture extrusion (long cooling die temperature [LCDT]: 40, 60 and 80 °C; screw speed [SS]: 300, 400 and 500 rpm) to obtain meat-mimicking fibrous meat analogues (FMAs). The results showed that OFC reduced the structural strength (e.g., hardness, chewiness) of the FMAs, whereas LCDT strengthened the structure. Microtomography imaging revealed that FMAs containing more OFC presented smaller void thickness, thus reducing the FMAs' water holding capacity. An in-vitro gastrointestinal model showed that the extractability and viscosity of β-glucan were well preserved, particularly at low LCDT. Overall, it was possible to add substantial amounts of OFC (30–50%) to FMAs while maintaining fibrous meat-mimicking structures and retaining the oat fiber's viscous properties.

1. Introduction

The adoption of an animal-free diet has increased drastically in the Western World, responding primarily to a greater awareness of greenhouse emissions from the meat and dairy industry. Compared to other food sources, beef production is responsible for the largest methane emissions, and aboveground changes in biomass due to deforestation (MacLeod, Hasan, Robb, & Mamun-Ur-Rashid, 2020; Poore & Nemecek, 2018). As plant-based meat analogues are gaining popularity, there is also a growing concern on the sustainable production and nutritional suitability of raw materials.

Industrially, high-moisture extrusion is the most cost-effective method to obtain fibrous meat analogues due to its various associated advantages: continuous process, versatility, compounding capacity and high-temperature short-time approach. According to various sources (Akdogan, 1999; Noguchi, 1989; Plattner, 2020), water incorporation in the production of meat analogues from popular grains (e.g., soybean) is usually around 60%. This could depend on the physicochemical characteristics of the flour used and the processing conditions (e.g., temperature profile). An essential accessory for the formation of fibrous structures is a long cooling die coupled with the last section of the barrel. The long cooling die allows the phase-separated proteins to align in the direction of the flow at cooling temperatures (below 100 °C), leading to the formation of protein/protein-based fibrous structures (Cheftel, Kitagawa, & Quéguiner, 1992). Soybean, pea and wheat are among the most common sources of protein isolates or concentrates used in the production of meat analogues (Plattner, 2020).

Plant ingredients could additionally offer great dietary prospects with the introduction of dietary fiber. Oat is a formidable cereal grain that would potentially (1) bring EFSA-approved health benefits on β-glucan (FDA, Food and Drug Administration, Department of Health and Human Services (HHS), 1997; EFSA Panel on Dietetic Products, 2009, EFSA Panel on Dietetic Products, 2010, EFSA Panel on Dietetic Products, 2011) and (2) confer greater physical functionality to the end-

Abbreviations: D-WHC, Water hydration capacity measured via destructive method; D-WSI, Water solubility index measured via destructive method; FMA, Fibrous meat analogue; LCDT, Long cooling die temperature; MLR, Multiple linear regression analysis; ND-OAC, Oil absorption capacity measured via non-destructive method; ND-WHC, Water hydration capacity measured via non-destructive method; OFC, Oat fiber concentrate; PLSR, Partial least squares regression; PPI, Pea protein isolate; Ten-A, Area under force-distance curve upon tensile cutting strength; Ten-P, Peak force upon tensile cutting strength; Tran-A, Area under force-distance curve upon transverse cutting strength; Tran-P, Peak force upon transverse cutting strength; WAI, Water absorption index; WSI, Water solubility index.

* Corresponding author at: University of Helsinki, P.O. Box 66, Agnes Sjöbergin katu 2, FI-00014, Finland.
E-mail address: jose.ramosdiaz@helsinki.fi (J.M. Ramos Diaz).

https://doi.org/10.1016/j.ifset.2022.102954
Received 25 December 2021; Received in revised form 6 February 2022; Accepted 16 February 2022
Available online 18 February 2022

Table 1
Chemical composition and physicochemical characterization of raw materials (oat fiber concentrate, *OFC*; pea protein isolate, *PPI*).

		Content (g/100 g d.m.)													
		Protein, %		Dietary fiber, %			Fat, %	[4]Starch, %	WAI		WSI		D*[3,2]*		D*[4,3]*	
				[1]soluble	insoluble	total										
OFC	100	24.8	±0.06	[2]20.8	[2]23.1	[2]43.9	[2]4.4	26.9	657.1[a]	±7.2	9.8[c]	±0.44	65.4[c]	±0.12	317.3[a]	±2.1
	70:30	40.4		15.6	17.3	32.9	5.8	20.9	489.5[b]	±16.9	14.4[b]	±1.2	70.5[b]	±3.4	271.3[b]	±2.1
OFC:PPI	50:50	56.0		10.4	11.6	22.0	6.7	15.3	435.2[c]	±10.4	18.2[a]	±1.8	74.2[ab]	±2.2	234.3[c]	±10.2
	30:70	71.5		5.2	5.8	11.0	7.6	9.9	444.2[c]	±12.7	17.0[a]	±1.9	74.6[ab]	±2.1	198.7[d]	±10.1
PPI	100	87.1	±0.00	n.d.	n.d.	[3]1	[3]9.0	2.9	352.8[d]	±15.1	18.3[a]	±1.2	75.2[a]	±1.5	137.3[e]	±2.1

Water absorption index, *WAI*; water solubility index, *WSI*; surface area moment mean, *D[3,2]*; volume moment mean, *D[4,3]*.
[1]Content of soluble dietary fiber in OFC measured as β-glucan; [2]Measurement conducted in duplicate; [3]Data provided by producer; [4]% Starch = 100 – (% protein + % dietary fiber + % fat).
[a-e]Different letters indicate significant difference at level p of 5%.

product (Ahmad, Anjum, Zahoor, Nawaz, & Dilshad, 2012). As reviewed by various authors (Mälkki & Virtanen, 2001; Tosh, 2013; Wood, 2010), the viscosity of β-glucan, resulting from its degree of solubility/extractability in water, explains the glucose-attenuating role of β-glucan. Evidence suggests that the viscosity of β-glucan is involved in the reduction of cholesterol levels (Othman, Moghadasian, & Jones, 2011; Wolever et al., 2010). When introducing β-glucan-rich oat ingredients to plant-based extrudates, the challenge is to maintain (i) the extractability of β-glucan upon physiological conditions and (ii) the functionality of β-glucan in small intestine conditions, thereby ensuring the health impacts of β-glucan. These properties of β-glucan can be studied in vitro by a gastrointestinal model, which further determines β-glucan's potential to influence the viscosity of the digesta (Mäkelä, Brinck, & Sontag-Strohm, 2020).

On the other hand, pea is a legume whose protein has been lately shown to be able to form meat-mimicking fibrous structures (Plattner, 2020). Osen, Toelstede, Wild, Eisner, and Schweiggert-Weisz (2014) tested different pea protein isolates for the development of fibrous meat analogues, and observed that textural properties (e.g., cutting strength) were heavily dependent on the temperature of the extruder's last section (prior to cooling die).

According to Yuliarti, Kovis, and Yi (2021), higher contents of pea protein isolate (up to 17% d.m.) increased the hardness and chewiness of meat analogues. These authors attributed the remarkable increase in structural strength to a more extensive network of protein cross-links. It is a common feature of extruded plant-protein-based meat analogue that the conformation of protein/protein-based fibrous structures is tight as juiciness and moisture retention reduces (Sha & Xiong, 2020).

By contrast, the addition of dietary fiber to high-protein-containing plant-based extrudates appears to disrupt internal structures (Leonard, Zhang, Ying, & Fang, 2020). Addition of oat fiber concentrate could contribute to a (i) stronger phase separation between plant proteins and (ii) higher moisture absorption linked to juiciness.

The aim of the present study was to investigate the formation of fibrous structures, resulting from the high-moisture extrusion (under various conditions) of blends containing oat fiber concentrate and pea protein isolate. This development seeks to enhance the nutritional profile of plant-based meat analogues through the increase of dietary fiber. Preservation of extractability and viscosity of β-glucan—as primary properties linked to its physiological functionality—was investigated using an in vitro gastrointestinal model. Assessment of the cause-effect relationship between process parameters and mechanical/physicochemical properties of FMAs was conducted.

2. Material and methods

2.1. Materials

Oat fiber concentrate (OFC) and pea protein isolate (PPI) were purchased from companies based in Finland and France, respectively. These companies used oat (*Avena sativa*) and pea (*Pisum sativum*) as raw materials. The analysis of protein content followed the Dumas combustion method (Vario MAX CN, Germany) using a nitrogen-to-protein conversion factor of 6.25. The content of total dietary fiber (including soluble and insoluble) was measured following the AOAC 991.43 method (AOAC Official Methods of Analysis, 2005), while soluble dietary fiber in OFC was measured as β-glucan using the AOAC 995.16 method (AOAC Official Methods of Analysis, 2005). Fat content was expressed as a sum of fatty acid methyl esters. Fat extraction was conducted with acetone using an ASE instrument (Dionex ASE-200, Dionex Corporation; Sunnyvale, CA) (Lampi et al., 2015). Lipids were methylated, and subsequently quantified with a gas chromatographic method according to Liu, Lampi, and Ertbjerg (2018). Chemical composition is expressed as dry matter (d.m.), as shown in Table 1.

The water absorption index (WAI) and water solubility index (WSI) of ingredients were measured following the method described by Dansby and Bovell-Benjamin (2003); deionized water was used as solvent. The particle diameter (of flours) was measured using a laser diffraction particle size analyzer (Mastersizer 3000 SM, Malvern Instruments Ltd., Worcestershire, UK) with a dry powder dispersion unit (Aero S); the refractive index was set at 1.46.

2.2. Extrusion process

FMAs were obtained at different OFC levels (25, 50, and 75% of solids), temperatures of long cooling die (LCDT: 40, 60, and 80 °C), and screw speeds (SS: 300, 400 and 500 rpm). The selection of these three independent variables and their range were based on preliminary experiments, whose aim was to secure structurally stable FMAs. Sample collection was done in line with a split-plot Box-Behnken experimental design (**Appendix A**). A twin-screw laboratory extruder (Thermo Prism PTW24, Thermo Haake, Polylab System, Germany; Fig. 1) coupled with a long cooling die (flat cooling noozle FKD75, DIL Deutsches Institut für Lebensmitteltechnik, Quakenbrück, Germany) was used to produce the FMAs. Reverse osmosis water was the only liquid ingredient fed into the extruder (60% water content), and the total feed rate was 85 g/min. The process was controlled through real-time measurement of torque (N.m) and pressure (bar) at section 7 (TS-D1; Fig. 1). Torque and pressure—corresponding to each period of sample collection—were computed as response variables for statistical analysis. Upon exit, the FMAs were cut into pieces of 20-cm in length and placed inside polyethylene ziplock bags for subsequent storage at −20 °C. For analyses, frozen FMAs were transferred to a cold room (5 °C) for overnight storage, and then kept at room temperature for 2 h.

2.3. Determination of mechanical and physicochemical properties

The mechanical properties of the FMAs were assessed using a Texture Analyzer TAXT2i (Stable Micro Systems, Surrey, England). In the *texture profile analysis* (TPA), the FMAs were cut into rectangular specimens

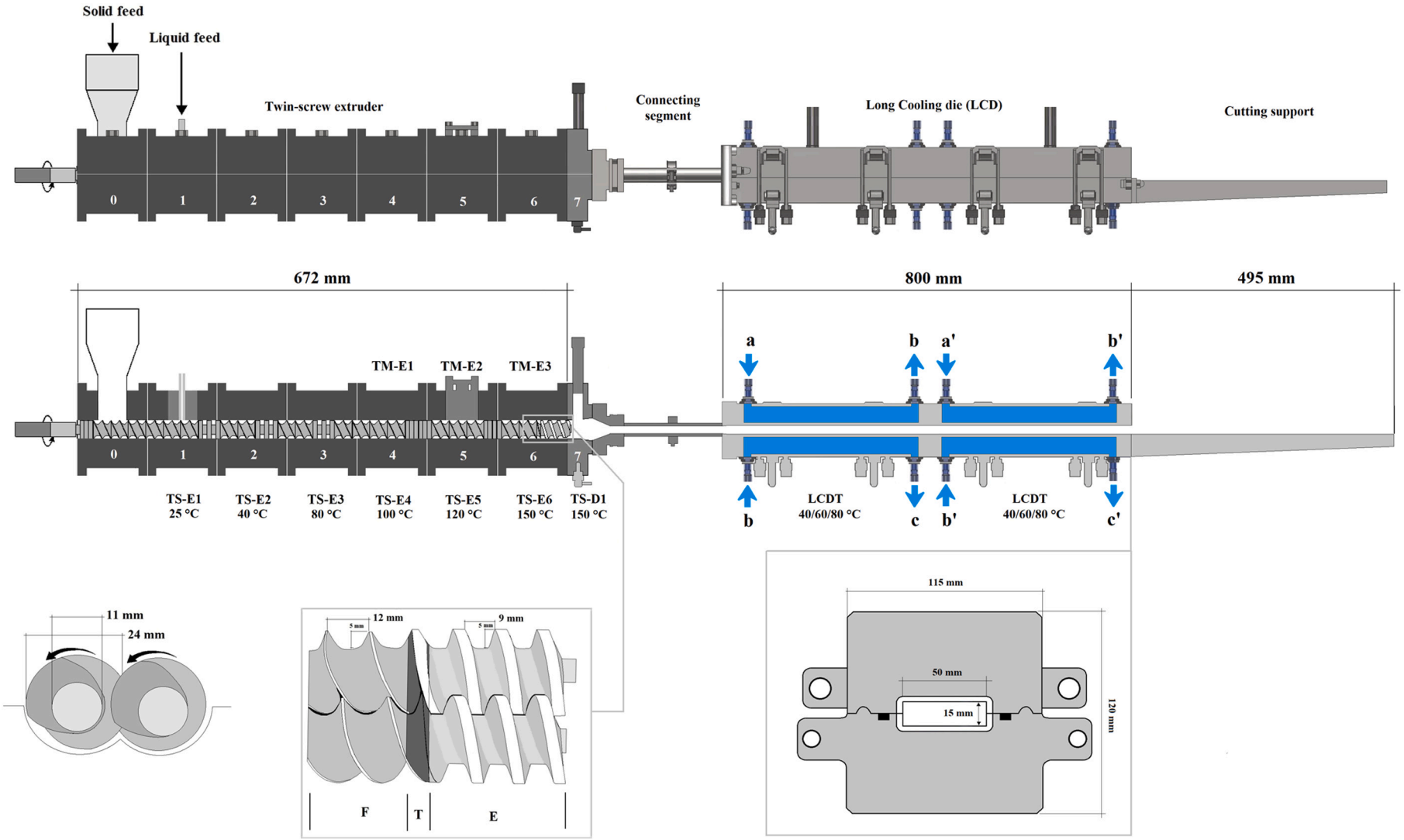

Fig. 1. Technical description of the twin-screw extruder and long cooling die used for the production of fibrous meat analogues containing OFC and PPI.

(five replicates; 24 mm [L] × 24 mm [W] × 14 mm [H]) and placed on a flat square aluminum sample holder. A cylindrical probe (Ø 36 mm)—fixed to the texture analyzer's mechanical arm—performed two sequential vertical descents on every specimen, while the corresponding data (i.e., force vs time) were registered. The settings were as follows: load cell, 30 kg; pre-test speed, 1 mm/s; test speed, 1 mm/s; post-test speed, 5 mm/s; deformation distance, 7 mm (50% strain); resting time, 5 s; and trigger force, 5 g. Each measurement resulted in a two-cycle force-time curve from which hardness, gumminess, springiness, and chewiness were calculated using the Eqs. (1)–(4), respectively.

$$\text{Hardness} = F_{max \rightarrow A_1} \tag{1}$$

$$\text{Gumminess} = \frac{A_2}{A_1} \times \text{Hardness} \tag{2}$$

$$\text{Springiness} = \frac{L_2}{L_1} \tag{3}$$

$$\text{Chewiness} = \text{gumminess} \times \text{springiness} \tag{4}$$

where A_1 or A_2 is the area to peak force corresponding to cycle 1 or cycle 2, respectively; $F_{\max \rightarrow A1}$ is the maximum force corresponding to area A_1; L_1 or L_2 is the length of time corresponding to A_1 or A_2, respectively. In the *cutting strength test*, samples were prepared following two cutting techniques: transverse and tensile (five replicates; **Appendix B**). A razor blade probe—fixed to the texture analyzer's mechanical arm—performed a three-point bending cut upon descent. The settings were: load cell, 5 kg; pre-test speed, 1 mm/s; test speed, 1 mm/s; post-test speed, 5 mm/s; and cutting distance, 10 mm. The collected data were: (1) area under force-time curve and (2) maximum force.

Prior to the measurement of the *water hydration capacity and water solubility index* via *a destructive method* (D-WHC; D-WSI), the FMAs were shredded and subsequently dried in an airflow convection oven (Termaks, Bergen, Norway) at 50 °C for 12 h. Dried samples were milled using an ultra-centrifugal mill (Retsch ZM 200, Haan, Germany) at 10,000 rpm, and stored in zip-lock plastic bags at room temperature (25 °C). D-WHC was measured following the AACC method 56–30 (AACC American Association of Cereal Chemists, 2010), while D-WSI measurement followed the method described by Dansby and Bovell-Benjamin (2003). In the measurement of the *water hydration/oil absorption capacity* via *a non-destructive method* (ND-WHC; ND-OAC), the FMAs were cut into pieces of the following dimensions: 20 mm × 30 mm × 10 mm, and dried in an airflow convection oven (Termaks, Bergen, Norway) at 40 °C for about 24 h. Each dried piece was weighed and immersed in 40 ml of Milli Q water or rapeseed oil (Keiju, Bunge Finland Ltd., Finland) (50-ml Eppendorf tube) at 50 °C (water bath) for 16 h, followed by draining for 5 min. ND-WHC or ND-OAC were expressed as grams of water/oil retained per gram of dried sample using Eq. (5),

$$ND\text{-WHC or NDOAC}(\%) = \frac{(W_{AR} - W_{BR})}{W_{BR}} \times 100 \tag{5}$$

where W_{AR} is the weight of the samples after rehydration and W_{BR} is the weight of the samples before rehydration. The color space parameters L*, a*, and b* were measured (L*: lightness; a*: redness; b*: yellowness) using a Minolta CR-400 Chroma Meter (Konica Minolta Sensing, Inc., Osaka, Japan) on the FMAs (prior to drying) prepared for the determination of ND-WHC or ND-OAC. The complete dataset is presented in **Appendix C**.

2.4. In vitro digestibility

The content, extractability (aka solubility) and viscosity of β-glucan were studied by an in vitro gastrointestinal model according to Mäkelä et al. (2020). The method models the physical state of β-glucan under the conditions of the small intestine, including the extractability of β-glucan and the changes in viscosity when concentrating the in vitro extracts by evaporation. The amount of the sample weighed for in vitro digestion was calculated to reach the theoretical β-glucan content of 0.6% (*w*/w) in the final in vitro extract, assuming a extractability of 100%. The final β-glucan concentration of the in vitro extract represented the potential of β-glucan to increase the consistency or viscosity of the intestinal digest during the path of digestion. Two repeated digestions were performed for the FMAs.

2.5. Imaging analysis of extrudate

FMAs were cut into pieces of defined volume (**Appendix B**, transverse) and freeze-dried (Lyovac GT 2, Amsco Finn-Aqua GmbH, Hürth, Germany) for 4 days. Freeze-dried FMAs were imaged with an X-ray micro-CT system phoenix nanotom|s (phoenix|x-ray Systems + Services GmbH, currently part of Waygate Technologies owned by Baker Hughes). The FMAs were placed in a small plastic cup and supported by Styrofoam balls to ensure immobility during the scan. The operating voltage was 60 kV and the current 150 μA, and no filter was used. Each FMA was imaged by taking 1600 projection images around 360° rotation, with a 3 × 500 ms exposure time for each projection. The pixel size in the images was 20 μm. The data was reconstructed into 3D volumes using the phoenix datos|x 2 reconstruction software version 2.4.0 (phoenix|x-ray Systems + Services GmbH). The image analysis was done in Fiji/ImageJ (Rueden et al., 2017; Schindelin et al., 2012). Noise was reduced by non-local means denoising (Buades, Coll, & Morel, 2011; Darbon, Cunha, Chan, Osher, & Jensen, 2008), and the void portion was then identified by manually choosing a threshold value (the same for all samples) below which the gray scale values were interpreted as belonging to the void space. The thickness distribution for the void space was calculated using the ImageJ LocalThickness plugin (Dougherty & Kunzelmann, 2007).

Selected FMAs were thawed (details in Section 2.2) and cut into pieces 5 cm in length. Minor cuts were performed on the samples to enforce sidewise opening and display. First, large pictures were taken with a digital single-lens reflex (DSLR) body (Nikon 7200, Tokyo, Japan) attached to a telephoto lens (18–400 mm f/3.5–6.3 DI II VC HLD -zoom-objective, Tamron Co., Ltd., Saitama, Japan) in a light-controlled cabinet (D50, warm daylight). The settings were: distance to object, 20 cm; magnification, 18 mm; aperture, 7.1; shutter speed, 250; and ISO, 1000. Raw images (unprocessed data) were processed with Corel PaintShop Pro (v. 2021, Corel Corporation, Ottawa, Canada). Second, the same samples were placed in a sample holder of a Stemi DV4 stereomicroscope (Carl Zeiss MicroImaging, Göttingen, Germany). The stereomicroscopic images were initially processed using Zeiss Zen software (Zeiss, Jena, Germany) and then with Corel PaintShop Pro.

2.6. Statistical analyses

The effect of OFC (30, 50, and 70% of solids), LCDT (40, 60 and 80 °C) and SS (300, 400, and 500 rpm) and their interactions on the mechanical and physicochemical properties of the FMAs were statistically analyzed via multiple linear regression (MLR) analysis and partial least squares regression (PLSR) modeling with MODDE (v. 12.1, Umetrics, Sweden) and SIMCA (v. 15.0, Umetrics, Sweden), respectively. For PLSR, some response variables (i.e., hardness, ND-WHC, D-WSI, Ten-A, and Tran-A) were omitted as they could not be successfully computed into the model thereby reducing the total percentage of explained variance. In terms of characterization of the raw materials, chemical analyses (i.e., content of dietary fiber, content of total fat) were mostly conducted in duplicate while mechanical/physicochemical analyses (e.g., WAI, WSI, particle size distribution) were conducted, at least, in triplicate.

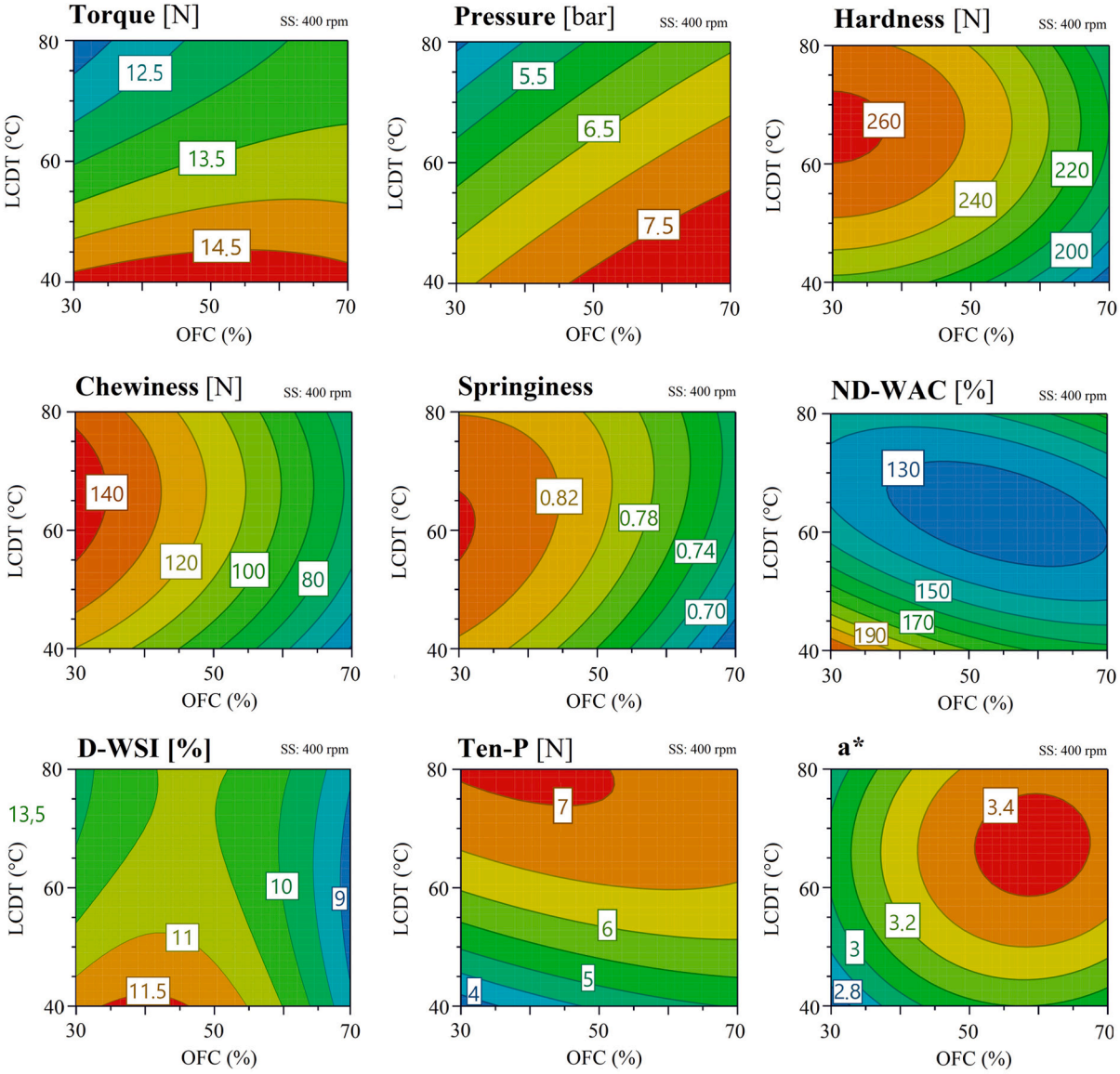

Fig. 2. Contour plots (2D) corresponding to process parameters and mechanical/physicochemical characteristics of fibrous meat analogues in line with the multiple linear regression modeling. Water hydration capacity measured via a non-destructive method, *ND-WHC*; peak force upon tensile cutting strength, *Ten-P*; redness, *a**.

3. Results and discussion

3.1. Characterization of raw materials

While PPI was the main source of protein in the FMAs formulated in this study, OFC served as a secondary source. Approximately one-fourth of OFC was protein (expressed as solids; Table 1). In flour blends, the calculated protein contents varied between 40 and 70% (of solids). OFC, by contrast, was the ingredient with the largest content of dietary fiber (from which half was soluble dietary fiber, β-glucan), while PPI showed negligible contents (Table 1). Higher OFC in flour blends reasonably increased the total content of dietary fiber and starch, as shown in Table 1. Almost one fourth of OFC was starch while PPI presented minimal contents (<5% of solids). In blends, starch was the third largest component after protein and dietary fiber (Table 1). Both PPI and OFC contained less than 10% fat; a modest content compared to other components (e.g., protein, dietary fiber). Regarding WAI and WSI, OFC almost doubled the WAI of PPI, contrary to the observation with WSI (Table 1). In flour blends, WAI decreased and WSI increased at lower OFC.

In terms of volume moment mean, D[4,3], the particles of OFC were almost two and a half times larger than those of PPI (Table 1). Conversely, the particle surface area moment mean, D[3,2], of OFC seemed smaller than those of PPI. Overall, OFC had a larger particle volume but a smaller surface area compared to PPI. Progressive changes in particle size were observed with increasing OFC (Table 1).

3.2. Effect of process parameters on FMAs

In general, LCDT was the process parameter with the greatest effect on the mechanical and physicochemical properties of the FMAs (Fig. 2). By contrast, SS had practically no effect. Changes in torque and pressure at the die were inversely proportional to LCDT (Table 2, Fig. 2). There is a possibility that a highly viscous melt inside the long cooling die (most probably associated with high LCDT) restricted the flow coming from the extruder, thus altering the recorded readings of pressure and torque in section 7 (Fig. 1).

Studies on the relationship between temperature and viscosity of starch-based materials generally suggest that increasing temperature effectively contributes to a reduction in the viscosity of the melt (Chang,

Table 2
Effects of independent variables (oat fiber concentrate, *OFC*; long cooling die temperature, *LCDT*; screw speed, *SS*) on processing parameters, and physicochemical/mechanical properties of meat analogues.

	Tor	Pre	Hard	Chew	Gum	Spring[a]	Non-destructive		Destructive		Cutting strength				L*[b]	a*	b*[b]
							WHC	OAC[b]	WHC[b]	WSI	Ten-P	Ten-A	Tran-P[b]	Tran-A[b]			
Constant	13.5	6.7	246.7	116.6	145.6	0.80	126.3	908.2	2.7	10.6	646.3	485.7	635.7	468.4	503.7	337.4	138.8
O: OFC	0.38*	0.79**	−261.8***	−341.6***	−342.3***	−0.06***	−802.0	335.3*	0.31	−0.72**	0.21	19.6	−0.34	−19.5	1.0*	0.17***	0.17
T: LCDT	−1.1***	−1.0***	133.3*	101.0*	108.5**	0.02	−160.5**	−317.6*	0.05	−0.40**	12.2***	8.9***	0.02	15.1	0.82	0.12***	0.20*
S: SS	0.15	0.09	156.5	−300.8	−165.4	−0.01	777.7	0.85	0.05	0.05	0.30	209.8	0.15	106.5	0.37	0.07**	0.15
*O*O*	−0.21	−0.17	−129.4	−727.9	−91.1*	−0.02	117.6	179.5	−0.06	−1.1	−0.21	−160.2	−0.35	−191.2	−0.09	−0.19***	−0.21
*T*T*	0.22	−0.13	−204.3*	−148.4**	−159.8**	−0.03	382.5***	516.2*	0.07	0.31	−0.66*	−539.9*	−0.32	−24.4	−0.29	−0.18***	−0.30*
*S*S*	−0.07	0.15	−626.5	−452.8	−210.1	−0.02	205.2	0.81	0.06	0.28	−0.003	0.04	0.07	13.2	0.20	0.05	0.14
*O*T*	0.37	0.23	0.71	122.2	0.87	0.02	207.1**	21.8	−0.05	0.39	−0.44	−318.5	0.01	−0.30	0.21	0.02	−0.08
*O*S*	−0.21	0.01	−635.8	−498.5	−361.1	−0.02	898.0	114.3	0.001	0.320	−0.63	−501.7	0.15	141.1	−0.32	−0.16***	−0.21
*T*S*	0.25	0.08	−100.7	−0.47	−135.3	0.01	−535.1	120.4	−0.14	−0.18	−0.20	−147.9	−0.37	−276.2	−0.24	0.02	−0.09
R^2	0.90	0.91	0.91	0.96	0.97	0.88	0.92	0.78	0.63	0.86	0.92	0.91	0.51	0.59	0.72	0.97	0.81
Q^2	0.61	0.47	0.41	0.76	0.85	0.03	0.27	−0.20	−0.65	0.43	0.49	0.47	−0.20	−0.20	−0.20	0.74	−0.20

Torque, *Tor*; pressure, *Pre*; hardness, *Hard*; chewiness, *Chew*; gumminess, *Gum*; springiness, *Spring*; water hydration capacity, *WHC*; oil absorption capacity, *OAC*; peak force upon tensile cutting strength, *Ten-P*; area under force-distance curve upon tensile cutting strength, *Ten-A*; peak force upon transverse cutting strength, *Tran-P*; area under force-distance curve upon transverse cutting strength, *Tran-A*; lightness, L*; redness, a*; yellowness, b*.

*, **, *** Significant at $p < 0.05$, $p < 0.01$ and $p < 0.001$.

[a] Regression was NOT significant ($p > 0.05$).

[b] Lack of fit was significant ($p < 0.05$).

Martinez-Bustos, Park, & Kokini, 1999; Gutkoski & El-Dash, 1999; Osen et al., 2014). In the present study, high-protein-containing melt (e.g., 30% OFC: 70% PPI) showed a bigger decrease in torque and pressure—at increasing LCDT—than high-fiber-containing melt (e.g., 70% OFC: 30% PPI) (Fig. 2). Regarding mechanical properties, LCDT had a direct effect on hardness, chewiness and, particularly, gumminess up to certain point (Table 2). As shown in Fig. 2, chewiness and hardness peaked around 60 °C, before a slight drop at close to 80 °C. Clearly, greater mechanical strength of protein-based FMA was associated with high LCDT. Schreuders et al. (2019) noted that high processing temperature (high-temperature conical shear cell) was directly proportional to the mechanical strength of meat analogues containing PPI and wheat gluten. In the present study, the acting mechanical force was perpendicular to the flow direction, suggesting that changes in mechanical strength (e.g., hardness, chewiness, gumminess) could be linked to the orientation of the fibrous structures.

In general, the structural capacity of the FMAs to absorb water (i.e., ND-WHC) decreased by almost 30% at LCDT close to 80 °C (Fig. 2). Based on the MLR model, large changes in ND-WHC were observed between 40 and 60 °C (Fig. 2). Theoretically, ND-WHC would strongly depend on the capillarity and polar sites interacting with water (Osen et al., 2014), temperature being a key factor for induced protein denaturation and its capacity to retain water. It is likely that, in the current study, a higher LCDT led to the formation of stronger protein crosslinks and/or protein-CHO interactions thereby reducing the availability of hydrophilic groups (e.g., −NH3+, COO−). Similar, structural anisotropy might have a negative impact on the formation of capillary vessels, which could translate to a lower capacity to absorb water.

The solubility of milled FMAs (i.e., D-WSI) seemed to reduce at higher LCDT (Table 2). This effect was noticeable yet not strongly consistent across different compositional levels. In view of the present results, it is logical to suggest that higher LCDT removed internal stress, thereby toughening protein-CHO structures (annealing) and, probably, reducing the capacity to dissolve in deionized water. Liu and Hsieh (2008) observed that increasing temperatures of long cooling die considerably reduced the presence of non-covalent bonds while maintaining covalent interactions. These interactions could have an influence on the hydrophilic character of the sample as water molecules may find less bindable moieties.

The considerable increase in cutting strength (i.e., Ten-P) was in direct proportion to LCDT (Table 2; Fig. 2). This could most probably indicate a change in the direction of the fibrous structures from a longitudinally to a perpendicularly aligned structural distribution. According to Osen et al. (2014), the increase in tensile cutting strength at higher processing temperatures is associated with the unraveling of bonding sites for further crosslinking. In the present study, it is believed that crosslinking (i.e., covalent bonding) and positioning of fibrous structures had a synergic role in the substantial increase of Ten-P. From a methodological perspective, using either peak force (Ten-P) or area (Ten-A) under the curve to assess cutting strength led us to comparable interpretations.

Seemingly, the FMAs became redder at higher LCDT. However, this may also depend on compositional aspects (Fig. 2). It is likely that higher temperatures at long-cooling-die point triggered a Maillard reaction in a protein-fiber-based melt.

The PLSR plot showing an overview of cause-effect relationships between independent and response variables is presented in Fig. 3. Clearly, SS, located at the center of the plot, exhibited a minimal effect on any processing parameters (i.e., torque and pressure) or mechanical/physicochemical properties. However, LCDT was beyond Hotelling's T-squared (HT^2) confidence level of 99% (Fig. 3, lower right-hand side). This suggests that LCDT had a remarkable inverse effect on pressure, torque, and oil absorption capacity (ND-OAC)—and to a much lesser extent—lightness and yellowness. By contrast, cutting strength (i.e., Ten-P) increased in line with LCDT. Chewiness and gumminess showed a minor positive association with LCDT.

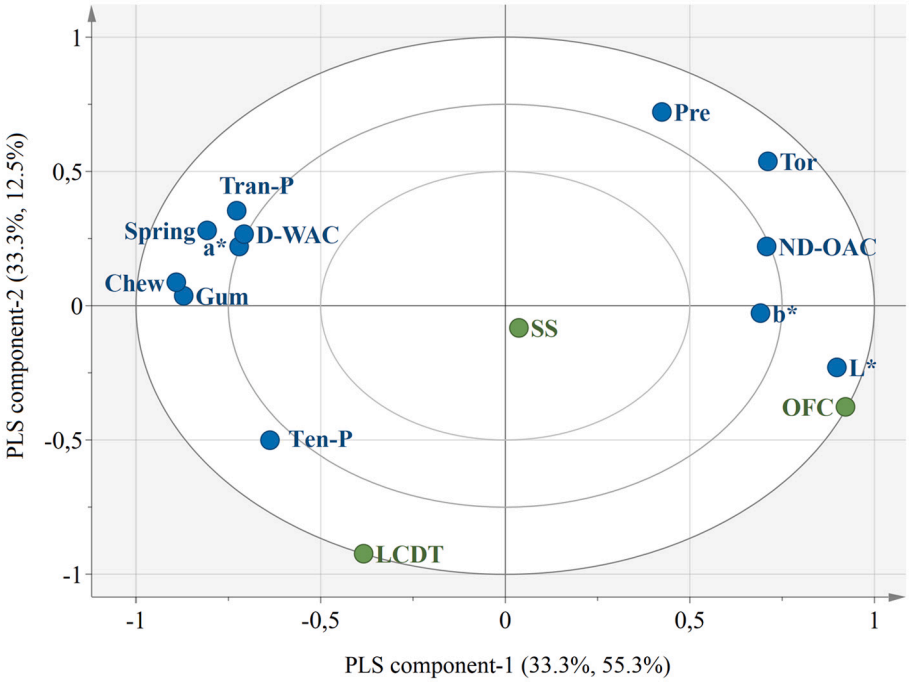

Fig. 3. Graphical representation of the partial least squares regression (PLSR) model. Independent variables are shown in green (content of oat fiber concentrate, *OFC*; long cooling die temperature, *LCDT*; screw speed, *SS*) while response variables are in blue (pressure, *Pre*; torque, *Tor*; chewiness, *Chew*; gumminess, *Gum*; springiness, *Spring*; non-destructive oil absorption capacity, *ND-OAC*; destructive water hydration capacity, *D-WHC*; peak force upon transverse cutting strength, *Tran-P*; peak force upon tensile cutting strength, *Ten-P*; lightness, *L**; redness, *a**; yellowness, *b**). The percentage variance explained by each PLSR component (1 and 2) is shown next to the adjacent axes. (For interpretation of the references to color in this figure legend, the reader is referred to the web version of this article.)

The PLSR plot also shows correlations among response variables. For instance, torque and pressure seemed to increase in line with ND-OAC while being inversely proportional to D-WAC. The abrasiveness of the process was probably associated with the FMAs' ability to absorb polar (water) or non-polar (oil) compounds. Additionally, Tran-P appeared to correlate with chewiness, gumminess and springiness; attributes associated with structural strength.

3.3. Role of protein and dietary fiber in FMAs

As described by the MLR models, OFC seemed to have a direct effect on torque and pressure; these changes seemed larger at higher LCDT (Table 2; Fig. 2). Although, some studies have claimed that the incorporation of protein isolate contributes to melt viscosity via stronger intermolecular reactions (Philipp, Emin, Buckow, Silcock, & Oey, 2018; Ralston & Osswald, 2008), β-glucan might have a comparable polymeric stabilization capacity, particularly in fiber-based systems (Choi, Seog, Kim, Park, & Lee, 2003).

The incorporation of OFC had an observable effect on the mechanical properties of the FMAs, such as hardness, chewiness, and gumminess (Table 2; Fig. 2). The weakening trend, shown in Fig. 2, can arguably be attributed to the presence of OFC in the FMAs. As expected, OFC (e.g., 70%) failed to fully substitute for the fibrous-forming pea protein component upon extrusion. However, the existence of a tenderness (defined as low biting effort; Purchas, 2014) 'sweet spot' between 30 and 50% OFC remains a possibility. The present study is consistent with the observation of De Angelis et al. (2020), who reported a two-fold decrease in hardness of meat analogues containing lower pea/oat protein content (from 78 to 55%). Overall, the results of the present study (hardness, 200–260 N) are roughly comparable to those of beef *M. semitendinosus* steak (199–270 N; Botinestean, Keenan, Kerry, & Hamil, 2016) and substantially higher than those of meat analogues made of soy protein concentrate (45–79 N; Chiang, Loveday, Hardacre, & Parker, 2019) (5 N; Zahari et al., 2020).

Regarding ND-WHC, OFC and LCDT had a combined effect (Table 2). At low LCDT (40–60 °C), more OFC (and less PPI) drastically reduced ND-WHC. De Angelis et al. (2020) reported higher water binding capacity (associated with the presence of polar molecules) in meat analogues containing more pea protein, which is in line with the present investigation. In fact, one may expect that the presence of β-glucan in OFC would axiomatically increase the water hydration capacity of meat analogues. Instead, this might have tightened fibrous structures thereby restricting the movement of water molecules across the capillary vessels. As observed in Fig. 4, the FMAs with low fiber content (30 OFC: 70 PPI) showed larger void areas than those containing high fiber content (70 OFC: 30 PPI). Although this perception was ambiguously reflected in porosity levels (Fig. 4), the assessment of void thickness seemed to confirm our visual observations; large void thickness was more likely to be present in FMAs with low fiber content (Fig. 5). This feature may have had an impact on the water uptake capacity of the FMAs.

Regarding D-WSI, increasing OFC noticeably reduced the amount of solubilized solids. This came as no surprise given the existence of soluble dietary fiber (i.e., β-glucan) in OFC and the high water content involved in extrusion. There is a chance that hydrocolloids such as β-glucan were able to preserve their molecular integrity during extrusion, thus contributing to the FMAs' water binding capacity.

The orientation of fibrous structures, derived from values of cutting strength (e.g., Ten-P), showed minor changes upon the increase in OFC, as shown in Fig. 2. Initially, it was expected that fibrous protein structures of high-protein-containing FMAs were more distinctive than those of high-fiber-containing FMAs. However, the formation of a layered fibrous structure was accomplished under all tested conditions. To the best of our knowledge, this is the first study where up to 33% dietary fiber—from which around half was β-glucan—was incorporated into FMAs with unprecedented success in the formation of anisotropic structures. Samard, Gu, and Ryu (2019) observed that an increase in protein (e.g., wheat gluten) had a direct effect on tensile cutting strength, which contradicts the current results.

Compositionally, the presence of insoluble dietary fiber in the FMAs was comparable to that of soluble dietary fiber. Unlike β-glucan, one would expect insoluble fiber to be abrasive upon the conformation of fibrous structures (Brennan, Monro, & Brennan, 2008; Ramos-Diaz et al., 2017). However, the water's lubricating effect (60% water content upon extrusion) might have prevented the disruptiveness of insoluble fiber.

According to the PLSR model (Fig. 3), OFC had a direct effect on the lightness and—to a lesser extent—yellowness of the FMAs. The discrepancy with the MLR model around redness (a*) can be resolved by

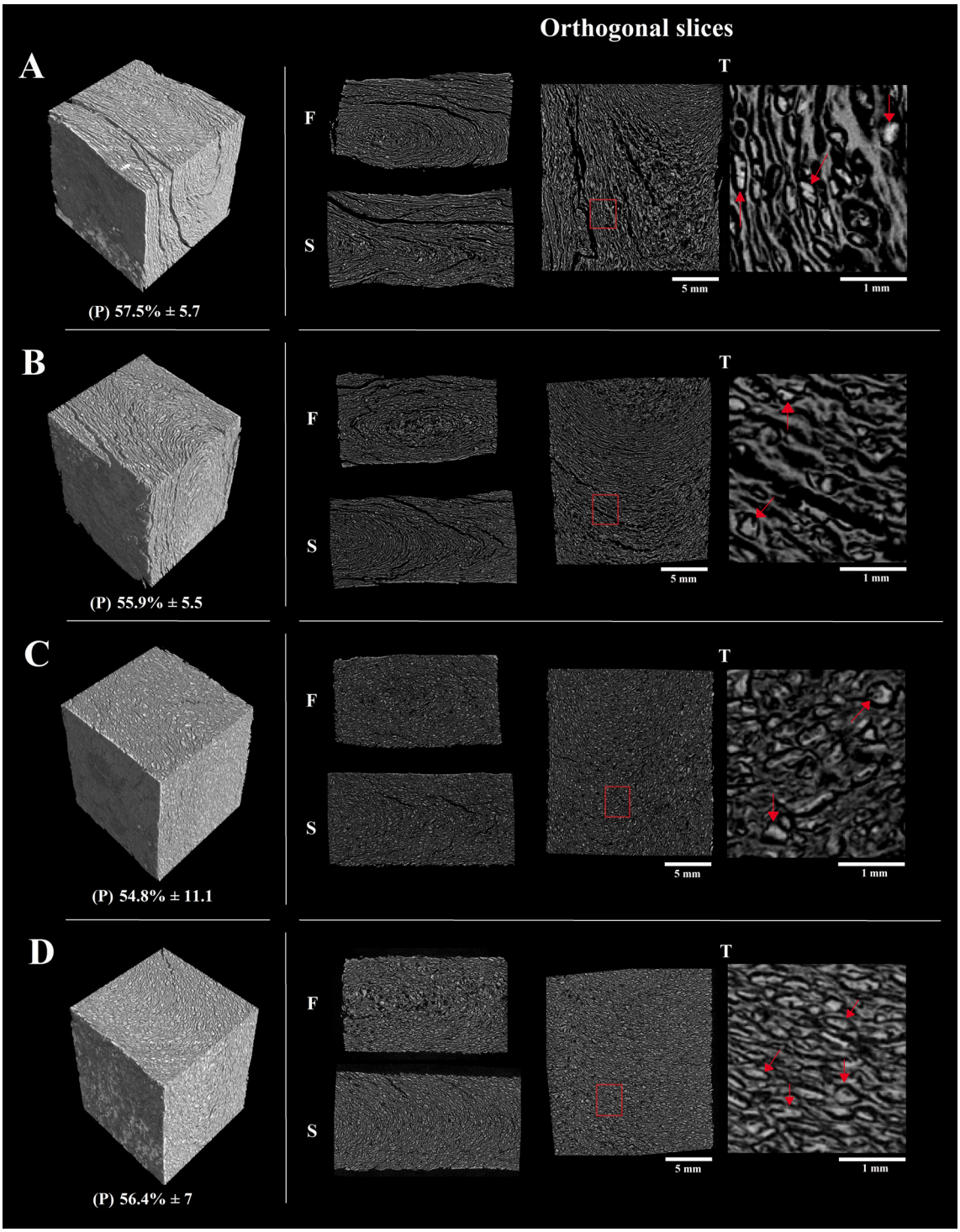

Fig. 4. MicroCT scans of fibrous meat analogues obtained at different flour ratios (OFC:PPI) and LCDT as follows: A. 30:70 and 40 °C; B. 30:70 and 80 °C; C. 70:30 and 40 °C; D. 70:30 and 80 °C. Porosity (P) is shown below each 3-D visualization (10 mm × 10 mm × 10 mm). Orthogonal slices from different view angles are shown: Front (F), Side (S), and Top (T). A few observed bodies fixated in fibrous structures are pointed at by red arrows. (For interpretation of the references to color in this figure legend, the reader is referred to the web version of this article.)

assessing the goodness of the model via the coefficient of determination (R^2) and coefficient of prediction (Q^2) (Table 2; **Appendix D**). Compared to PLSR, the MLR model for redness showed a remarkably better fit to the observed data. Thus, our results suggested that redness increased at higher OFC, as shown in Fig. 2. The changes in color were probably associated with the initiation and propagation of the Maillard reaction during processing.

In line with the MLR, the PLSR model showed a strong inverse effect of OFC on gumminess and chewiness, and also on springiness. The latter clearly reduced at higher OFC (in line with the proposed yet not significant MLR model; Fig. 2). In this study, the springiness of fiber-containing FMAs was substantially lower than that of FMAs containing soy protein concentrate (0.99; Zahari et al., 2020). To a certain degree, the loss of springiness could be linked to greater tenderness and palatability. Transverse cutting strength (i.e., Tran-P) was observed to be inversely proportional to OFC (possibly β-glucan). Theoretically, this

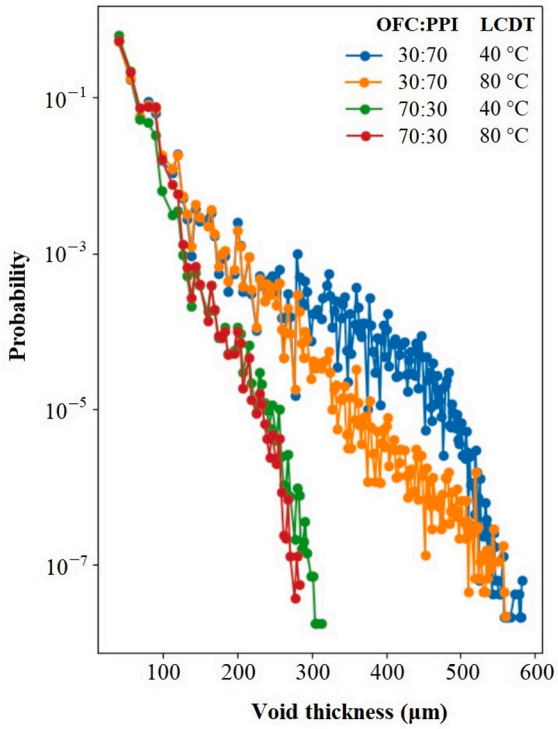

Fig. 5. Void thickness probability distribution in fibrous meat analogues obtained at two OFC:PPI (30:70 and 70:30) ratios and two LCDT (40 and 80 °C).

suggests that transverse cutting found greater resistance associated with perpendicularly oriented structures in low-fiber-containing FMAs (e.g., 30 OFC: 70 PPI). In high-fiber-containing FMAs (e.g., 70 OFC: 30 PPI), it is likely that fibrous structures aligned with the cutting direction thereby showing a lesser resistance to deformation. This agrees with the observation of Osen (2017) who also noticed that a perpendicular cutting force to the visible fibers (obtained from PPI) was consistently higher than a parallel cutting force.

Lastly, OFC had a presumable positive effect on ND-OAC, and a negative effect on D-WHC and Ten-P. A key point to note is that the Q^2 corresponding to ND-OAC, D-WHC and Ten-P was below 0.4.

3.4. Formation of fibrous structures in FMAs

Microtomography images of selected FMAs are shown in Fig. 4. In general, fibrous structures were more noticeable in FMAs with higher content of PPI (i.e., 30 OFC: 70 PPI) (Fig. 4A–B). Additionally, quasi-spherical bodies were observed in every tested sample, particularly in those containing more OFC (Fig. 4; see arrows pointing at the bodies). There is a possibility that those bodies—positioned between proteinaceous fibrous structures—are remnants of protein-fiber complexes or dietary fiber (clearly observed in Fig. 4A). To the best of our knowledge, this is the first time this structural phenomenon was observed in meat analogues involving high fiber content. In fact, as the content of β-glucan increased, fibrous structures appeared less defined, and the overall structure was more densely packed (i.e., 70 OFC: 30 PPI) (Fig. 4C-D). Arufe et al. (2017) observed that the progressive incorporation of soluble fiber into wheat flour doughs led to changes in bread porosity and porous structures, mainly governed by density. The present study could roughly relate to Arufe et al. (2017) as our FMAs seemed to have lower porosity at higher OFC (Fig. 4A-C).

Another potential explanation for the presence of bodies amid fibrous structures (Fig. 4) would be insoluble fiber. As discussed earlier, the typical disruptive character of insoluble fiber (Ramos-Diaz et al., 2017) was probably mitigated by the large water content used during high-moisture extrusion. This, however, might not have prevented the inert fixation of solids in-between structures.

Based on the assessment of void fraction (Fig. 5), FMAs with low fiber content (i.e., 30 OFC: 70 PPI) were strongly linked to a large void thickness (maximum between 500 and 600 μm), whereas the opposite occurred (maximum around 300 μm) with high-fiber containing FMAs (i.e., 70 OFC: 30 PPI). There is a possibility that substantial amounts of oat fiber (70 OFC: 30 PPI), particularly β-glucan, trapped free water that would otherwise be located between proteinaceous fibrous structures (30 OFC: 70 PPI). This would reasonably lead to smaller void fractions as observed in Fig. 5. Further, high-fiber-containing FMAs showed similar void thickness at changing LCDT, whereas low-fiber containing FMAs showed a greater chance of thicker void at 40 °C than at 80 °C (LCDT) (Fig. 5).

From the tested FMAs, those containing more PPI (30 OFC: 70 PPI) and produced at 40 °C (LCDT) showed a predominantly longitudinal arrangement of fibrous structures in relation to the melt flow (top and side view; Fig. 4A). Upon tearing (**Appendix E**, a-b), such FMAs displayed a predominant bell-shaped longitudinal orientation. Conversely, FMAs with similar composition (30 OFC: 70 PPI) produced at 80 °C showed a more curved perpendicular arrangement of fibrous structures in relation to the melt flow, particularly at the geometric center (top and side view; Fig. 4B). Such changes in the orientation of fibrous structures as a function of LCDT were initially assessed via tensile/transverse cutting strength (Fig. 2), and now visually confirmed via microtomography (Fig. 4) and tearing (**Appendix E**, a-d). According to Schreuders et al. (2021), the elasticity of PPI (observed via the Lissajous curve of stress versus strain amplitude) showed a considerable increase only when cooling (30 °C) was applied. The proneness to longitudinal alignment of fibrous structures at long cooling die could be a sign of elasticity, mostly observed at 40 °C (LCDT) (Fig. 4A).

At higher OFC (70 OFC: 30 PPI), differences in fibrous structures between FMAs produced at 40 or 80 °C (LCDT) were less pronounced. Despite this, the geometric center of FMAs (70 OFC: 30 PPI) produced at 40 °C (LCDT) (Fig. 4C) seemed to present slightly larger cavities (interpreted from the presence of dim gray to black areas) than those produced at 80 °C (LCDT) (Fig. 4D). Additionally, the magnified images corresponding to Fig. 4C and D seemed to reveal a more pronounced structural alignment for FMAs produced at 80 °C. Thus, it is logical to assume that high LCDT (i.e., 80 °C) could favor the formation of fibrous structures containing high contents of dietary fiber (i.e., 70 OFC:30PPI). In **Appendix E** (e–f), FMAs containing more OFC (70 OFC: 30 PPI) showed greater fragility upon tearing. The structural damage inflicted upon fibrous structures was even more noticeable at 40 °C (LCDT), which is consistent with characteristics observed in Fig. 4. Even though it comes as no surprise that the presence of 33% of dietary fiber (Table 1) disrupted the formation of fibrous structures, it is compelling to see that extrudates were relatively homogeneous.

3.5. In vitro digestibility of β-glucan

The β-glucan content in the FMAs increased in direct proportion to OFC addition, varying from 3 to 8% of fresh weight. The in vitro digestibility, or the extractability of β-glucan—determined using physiological conditions at 37 °C—was between 30 and 40% of the total β-glucan content in the FMAs. The FMAs with the most β-glucan (70 OFC: 30 PPI), and produced at 40 °C (LCDT), showed the highest degree of extractability (around 39%), while those produced at 80 °C (LCDT) showed the lowest degree of extractability (around 32%). Moriartey, Temelli, and Vasanthan (2011) observed that the extractability of β-glucan was considerably reduced at higher storage temperatures. The authors suggested potential interactions between β-glucan and amylose, or complexing among β-glucan molecules. In the present study, tighter structural alignments—shown in the microtomography images for FMAs produced at 80 °C (LCDT)—could have contributed to the smaller extractability of β-glucan during the in vitro digestion.

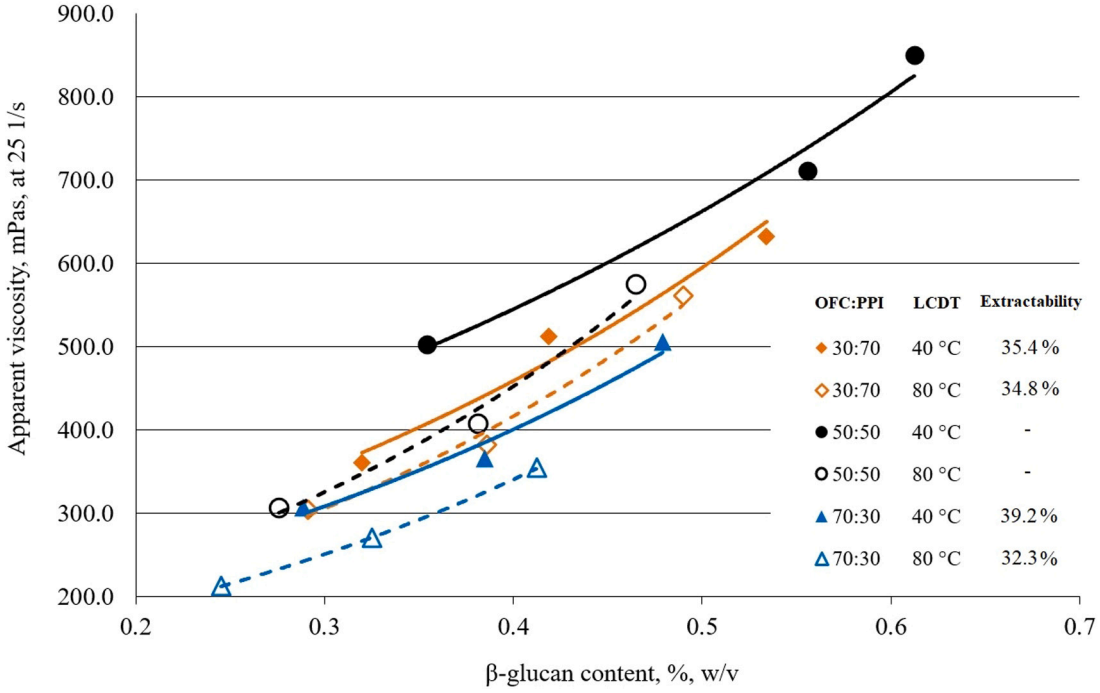

Fig. 6. The viscosity profiles of in vitro gastrointestinal model extracts from fibrous meat analogues (FMAs) containing various ratios of OFC and PPI (30:70, 50:50 and 70:30). FMAs were obtained at two LCDT, 40 and 80 °C.

The viscosity properties of β-glucan, present in the FMAs, were found to be well preserved after extrusion as the viscosity curve of in vitro extracts increased consistently with β-glucan concentration (30–50% OFC; Fig. 6). Using the same in vitro extraction method, Mäkelä et al. (2020) showed that, in commercial samples of oat-containing meat analogs, oat β-glucan was unable to produce a viscosity curve during concentration, except for one sample. The reason for this was unclear given the confidentiality of processing parameters. In any case, the viscosity curve of commercial meat analogs showed a slower increase in viscosity during β-glucan concentration, compared to the viscosity curves of the FMAs formulated herein. In the present study, the viscosity curve was observed to increase consistently at lower LCDT (at 40 °C compared with 80 °C; Fig. 6). Temperature-triggered structural changes (maybe polymeric interactions) may have altered the physicochemical properties of β-glucan, thereby changing extractability and, subsequently, viscosity in the in vitro extracts of the FMAs. To summarize, the use of substantial amounts of OFC (30–50%) to form FMAs was possible while retaining oat fiber's viscous properties.

4. Conclusions

The present study proved that it is possible to incorporate substantial amounts of soluble and insoluble dietary fiber and still obtain FMAs with different mechanical and physicochemical properties. Higher OFC reduced the mechanical strength (e.g., hardness, chewiness, springiness) and decreased the void fraction in the FMAs, while higher LCDT was associated with quantifiable changes in the orientation of fibrous structures (perpendicular proneness), smaller void thickness (at low OFC) and lower water update capacity across the FMAs. The observable quasi-spherical bodies physically sealed between fibrous structures could be remnants of dietary fiber or protein-fiber complexes. Upon in vitro gastrointestinal modeling, β-glucan (from OFC) showed well-preserved viscosity properties in the FMAs; however, some variation in extractability of β-glucan (between 30 and 40%) was observed. Lower LCDT was linked to higher extractability of β-glucan (39%). This study represents remarkable progress in the development of plant-based meat analogues with added health value.

CRediT authorship contribution statement

J.M. Ramos Diaz: Conceptualization, Methodology, Writing – original draft, Investigation, Formal analysis. **K. Kantanen:** Investigation, Formal analysis. **J.M. Edelmann:** Investigation, Formal analysis. **H. Suhonen:** Investigation, Formal analysis, Supervision. **T. Sontag-Strohm:** Conceptualization, Methodology, Writing – review & editing. **K. Jouppila:** Conceptualization, Methodology, Supervision, Writing – review & editing. **V. Piironen:** Conceptualization, Methodology, Supervision, Writing – review & editing.

Declaration of Competing Interest

Please check the following as appropriate:

- All authors have participated in (a) conception and design, or analysis and interpretation of the data; (b) drafting the article or revising it critically for important intellectual content; and (c) approval of the final version.
- This manuscript has NOT been submitted to, nor is under review at, another journal or other publishing venue.
- The authors have NO affiliation with any organization with a direct or indirect financial interest in the subject matter discussed in the manuscript.

Acknowledgements

This work has been funded by 3TexVegS+H, supported by European Institute of Innovation and Technology (EIT) and Leg4Life project, supported by the Strategic Research Council at the Academy of Finland (grant number 327698).

Appendix A. Supplementary data

Supplementary data to this article can be found online at https://doi.org/10.1016/j.ifset.2022.102954.

References

AACC American Association of Cereal Chemists. (2010). *International approved Methods of analysis, AACC International* (11th ed.). Minnesota: St. Paul.

Ahmad, A., Anjum, F. M., Zahoor, T., Nawaz, H., & Dilshad, S. M. R. (2012). Beta glucan: A valuable functional ingredient in foods. *Critical Reviews in Food Science and Nutrition, 52*(3), 201–212. https://doi.org/10.1080/10408398.2010.499806

Akdogan, H. (1999). High moisture food extrusion. *International Journal of Food Science and Technology, 34*, 195–207. https://doi.org/10.1046/j.1365-2621.1999.00256.x

AOAC Official Methods of Analysis. (2005). *AOAC international* (18th ed.). Maryland: Gaithersburg.

Arufe, S., Chiron, H., Dore, J., Savary-Auzeloux, I., Saulnier, L., & Della Valle, G. (2017). Processing & rheological properties of wheat flour dough and bread containing high levels of soluble dietary fibres blends. *Food Research International, 97*, 123–132. https://doi.org/10.1016/j.foodres.2017.03.040

Botinestean, C., Keenan, D. F., Kerry, J. P., & Hamil, R. M. (2016). The effect of thermal treatments including sous-vide, blast freezing and their combinations on beef tenderness of M. semitendinosus steaks targeted at elderly consumers. *LWT- Food Science and Technology, 74*, 154–159. https://doi.org/10.1016/j.lwt.2016.07.026

Brennan, M. A., Monro, J. A., & Brennan, C. S. (2008). Effect of inclusion of soluble and insoluble fibres into extruded beakfast cereal products made with reverse screw configuration. *International Journal of Food Science and Technology, 43*, 2278–2288. https://doi.org/10.1111/j.1365-2621.2008.01867.x

Buades, A., Coll, B., & Morel, J.-M. (2011). Non-local means denoising. *Image Processing On Line, 1*, 208–212. https://doi.org/10.5201/ipol.2011.bcm_nlm

Chang, Y. K., Martinez-Bustos, F., Park, T. S., & Kokini, J. L. (1999). The influence of specific mechanical energy on cornmeal viscosity measured by an on-line system during twin-screw extrusion. *Brazilian Journal of Chemical Engineering, 16*, N/A. https://doi.org/10.1590/S0104-66321999000300007

Cheftel, J. C., Kitagawa, M., & Quéguiner, C. (1992). New protein texturization processes by extrusion cooking at high moisture levels. *Food Reviews International, 8*, 235–275. https://doi.org/10.1080/87559129209540940

Chiang, J. H., Loveday, S. M., Hardacre, A. K., & Parker, M. E. (2019). Effects of soy protein to wheat gluten ratio on the physicochemical properties of extruded meat analogues. *Food Structure, 19*, 100–102. https://doi.org/10.1016/j.foostr.2018.11.002

Choi, H.-D., Seog, H.-M., Kim, S.-R., Park, Y.-K., & Lee, C.-H. (2003). Effect of β-glucan on gelatinization of barley starch. *Korean Journal of Food Science and Technology, 35*, 545–550. https://www.koreascience.or.kr/article/JAKO200304637331158.

Dansby, M. Y., & Bovell-Benjamin, A. C. (2003). Physical properties and sixth graders' acceptance of an extruded ready-to-eat sweetpotato breakfast cereal. *Journal of Food Science, 68*, 2607–2612. https://doi.org/10.1111/j.1365-2621.2003.tb07069.x

Darbon, J., Cunha, A., Chan, T., Osher, S., & Jensen, G. (2008). Fast nonlocal filtering applied to electron cryomicroscopy. In *Proceeding published in 5th IEEE International Symposium on Biomedical Imaging: From Nano to Macro. Paris, France*. https://doi.org/10.1109/ISBI.2008.4541250

De Angelis, D., Kaleda, A., Pasqualone, A., Vaikma, H., Tamm, M., Tammik, M.-L., Squeo, G., & Summo, C. (2020). Physicochemical and sensorial evaluation of meat analogues produced from dry-fractionated pea and oat proteins. *Foods, 9*, 1754. https://doi.org/10.3390/foods9121754

Dougherty, R. P., & Kunzelmann, K.-H. (2007). Computing local thickness of 3D structures with ImageJ. *Microscopy and Microanalysis, 13*, 1678–1679. https://doi.org/10.1017/S1431927607074430

EFSA Panel on Dietetic Products, Nutrition and Allergies (NDA). (2009). Scientific opinion on the substantiation of health claims related to beta glucans and maintenance of normal blood cholesterol concentrations (ID 754, 755, 757, 801, 1465, 2934) and maintenance or achievement of a normal body weight (ID 820, 823) pursuant to article 13(1) of regulation (EC) no 1924/2006. *EFSA Journal, 7*, 1254. https://doi.org/10.2903/j.efsa.2009.1254

EFSA Panel on Dietetic Products, Nutrition and Allergies (NDA). (2010). Scientific opinion on the substantiation of a health claim related to oat beta-glucan and lowering blood cholesterol and reduced risk of (coronary) heart disease pursuant to article 14 of regulation (EC) no 1924/2006. *EFSA Journal, 8*, 1885. https://doi.org/10.2903/j.efsa.2010.1885

EFSA Panel on Dietetic Products, Nutrition and Allergies (NDA). (2011). Scientific opinion on the substantiation of health claims related to oat and barley grain fibre and increase in faecal bulk (ID 819, 822) pursuant to article 13(1) of regulation (EC) no 1924/2006. *EFSA Journal, 9*, 2249. https://doi.org/10.2903/j.efsa.2011.2249

FDA, Food and Drug Administration, Department of Health and Human Services (HHS). (1997). Food labelling: Health claims; oats and coronary heart disease. *Final Rule. Federal Register, 62*(15), 3584–3601. https://www.federalregister.gov/documents/1997/01/23/97-1598/food-labeling-health-claims-oats-and-coronary-heart-disease.

Gutkoski, L. C., & El-Dash, A. A. (1999). Effect of extrusion process variables on physical and chemical properties of extruded oat products. *Plant Foods for Human Nutrition, 54*, 315–325. https://doi.org/10.1023/A:1008101209353

Lampi, A. M., Damerau, A., Li, J., Moisio, T., Partanen, R., Forssell, P., & Piironen, V. (2015). Changes in lipids and volatile compounds of oat flours and extrudates during processing and storage. *Journal of Cereal Science, 62*, 102–109. https://doi.org/10.1016/j.jcs.2014.12.011

Leonard, W., Zhang, P., Ying, D., & Fang, Z. (2020). Application of extrusion technology in plant food processing byproducts: An overview. *Comprehensive Reviews in Food Science and Food Safety, 19*, 218–246.

Liu, K., & Hsieh, F.-H. (2008). Protein–protein interactions during high-moisture extrusion for fibrous meat analogues and comparison of protein solubility methods using different solvent systems. *Journal of Agriculture and Food Chemistry, 56*, 2681–2687. https://doi.org/10.1021/jf073343q

Liu, M., Lampi, A. M., & Ertbjerg, P. (2018). Unsaturated fat fraction from lard increases the oxidative stability of minced pork. *Meat Science, 143*, 87–92. https://doi.org/10.1016/j.meatsci.2018.04.028

MacLeod, M. J., Hasan, M. R., Robb, D. H. F., & Mamun-Ur-Rashid, M. (2020). Quantifying greenhouse gas emissions from global aquaculture. *Scientific Reports, 10*, 11679. https://doi.org/10.1038/s41598-020-68231-8

Mäkelä, N., Brinck, O., & Sontag-Strohm, T. (2020). Viscosity of β-glucan from oat products at the intestinal phase of the gastrointestinal model. *Food Hydrocolloids, 100*, Article 105422. https://doi.org/10.1016/j.foodhyd.2019.105422

Mälkki, Y., & Virtanen, E. (2001). Gastrointestinal effects of oat bran and oat gum, a review. *LWT- Food Science and Technology, 34*, 337–347. https://doi.org/10.1006/fstl.2001.0795

Moriartey, S., Temelli, F., & Vasanthan, T. (2011). Effect of storage conditions on the solubility and viscosity of β-glucan extracted from bread under *in vitro* conditions. *Journal of Food Science, 76*, C1–C7. https://doi.org/10.1111/j.1750-3841.2010.01920.x

Noguchi, A. (1989). High moisture protein foods. In C. Mercier, P. Linko, & J. M. Harper (Eds.), *Extrusion cooking* (pp. 343–370). American Association of Cereal Chemists.

Osen, R. (2017). *Texturization of pea protein isolates using high moisture extrusion cooking*. Doctoral dissertation. Technische Universität München http://mediatum.ub.tum.de/?id=1356359.

Osen, R., Toelstede, S., Wild, F., Eisner, P., & Schweiggert-Weisz, U. (2014). High moisture extrusion cooking of pea protein isolates: Raw material characteristics, extruder responses, and texture properties. *Journal of Food Engineering, 127*, 67–74. https://doi.org/10.1016/j.jfoodeng.2013.11.023

Othman, R. A., Moghadasian, M. H., & Jones, P. J. H. (2011). Cholesterol-lowering effects of oat β-glucan. *Nutrition Reviews, 69*, 299–309. https://doi.org/10.1111/j.1753-4887.2011.00401.x

Philipp, C., Emin, M. A., Buckow, R., Silcock, P., & Oey, I. (2018). Pea protein-fortified extruded snacks: Linking melt viscosity and glass transition temperature with expansion behavior. *Journal of Food Engineering, 217*, 93–100. https://doi.org/10.1016/j.jfoodeng.2017.08.022

Plattner, B. (2020). Extrusion techniques for meat analogues. *Cereal Foods World, 65*, N/A. https://doi.org/10.1094/CFW-65-4-0043

Poore, J., & Nemecek, T. (2018). Reducing food's environmental impacts through producers and consumers. *Science, 360*, 987–992. https://doi.org/10.1126/science.aaq0216

Purchas, R. W. (2014). Tenderness measurement. In M. Dikeman, & C. Devine (Eds.), *Encyclopedia of meat sciences* (pp. 452–459). Netherlands: Academic Press, Elsevier.

Ralston, B. E., & Osswald, T. A. (2008). Viscosity of soy protein plastics determined by screw-driven capillary rheometry. *Journal of Polymers and the Environment, 16*, 169–176. https://doi.org/10.1007/s10924-008-0098-3

Ramos-Diaz, J. M., Sundarrajan, L., Kariluoto, S., Lampi, A.-M., Tenitz, S., & Jouppila, K. (2017). Partial least squares regression modelingof physical and chemical properties of corn-b asedsnacks containing kañiwa and lupine. *Journal of Food Process Engineering, 40*, Article e12396. https://doi.org/10.1111/jfpe.12396

Rueden, C. T., Schindelin, J., Hiner, M. C., DeZonia, B. E., Walter, A. E., Arena, E. T., & Eliceiri, K. W. (2017). ImageJ2: ImageJ for the next generation of scientific image data. *BMC Bioinformatics, 18*, 529. https://doi.org/10.1186/s12859-017-1934-z

Samard, S., Gu, B.-Y., & Ryu, G.-H. (2019). Effects of extrusion types, screw speed and addition of wheat gluten on physicochemical characteristics and cooking stability of meat analogues. *Journal of the Science of Food and Agriculture, 99*, 4922–4931. https://doi.org/10.1002/jsfa.9722

Schindelin, J., Arganda-Carreras, I., Frise, E., Kaynig, V., Longair, M., Pietzsch, T., … Cardona, A. (2012). Fiji: An open-source platform for biological-image analysis. *Nature Methods, 9*, 676–682. https://doi.org/10.1038/nmeth.1985

Schreuders, F. K. G., Dekkers, B. L., Bodnár, I., Erni, P., Boom, R. M., & van der Goot, A. J. (2019). Comparing structuring potential of pea and soy protein with gluten for meat analogue preparation. *Journal of Food Engineering, 261*, 32–39. https://doi.org/10.1016/j.jfoodeng.2019.04.022

Schreuders, F. K. G., Sagis, L. M. C., Bodnár, I., Erni, P., Boom, R. M., & van der Goot, A. J. (2021). Mapping the texture of plants protein blends for meat analogues. *Food Hydrocolloids, 118*, Article 106753. https://doi.org/10.1016/j.foodhyd.2021.106753

Sha, L., & Xiong, Y. L. (2020). Plant protein-based alternatives of reconstructed meat: Science, technology, and challenges. *Trends in Food Science & Technology, 102*, 51–61. https://doi.org/10.1016/j.tifs.2020.05.022

Tosh, S. (2013). Review of human studies investigating the post-prandial blood-glucose lowering ability of oat and barley food products. *European Journal of Clinical Nutrition, 67*, 310–317. https://doi.org/10.1038/ejcn.2013.25

Wolever, T. M. S., Tosh, S. M., Gibbs, A. L., Brand-Miller, J., Duncan, A. M., Hart, V., … Wood, P. J. (2010). Physicochemical properties of oat β-glucan influence its ability to reduce serum LDL cholesterol in humans: A randomized clinical trial. *The American Journal of Chemical Nutrition, 92*, 723–732. https://doi.org/10.3945/ajcn.2010.29174

Wood, P. J. (2010). Oat and rye β-glucan: Properties and function(review). *Cereal Chemistry, 315–330*. https://doi.org/10.1094/CCHEM-87-4-0315

Yuliarti, O., Kovis, T. J. K., & Yi, N. J. (2021). Structuring the meat analogue by using plant-based derived composites. *Journal of Food Engineering, 288*, Article 110138. https://doi.org/10.1016/j.jfoodeng.2020.110138

Zahari, I., Ferawati, F., Helstad, A., Ahlström, C., Östbring, K., Rayner, M., & Purhagen, J. K. (2020). Development of high moisture meat analogues with hemp and soy protein using extrusion cooking. *Foods, 9*, 772. https://doi.org/10.3390/foods9060772